Supporting Information for

Electrolyte-Mediated Assembly of Charged Nanoparticles

Sumit Kewalramani,[†] Guillermo I. Guerrero-García,[†,‡] Liane M. Moreau,[†] Jos W. Zwanikken,[†] Chad A. Mirkin,[†,§] Monica Olvera de la Cruz,[†,§,⊥,*] Michael J. Bedzyk,[†,⊥,*].

[†]Materials Science and Engineering Department, Northwestern University, Evanston, Illinois 60208, U.S.A.

[‡]Instituto de Física, Universidad Autónoma de San Luis Potosí, Àlvaro Obregón 64, 78000 San Luis Potosí, San Luis Potosí, Mexico.

[§]Department of Chemistry, Northwestern University, Evanston, Illinois 60208, U.S.A.

[⊥]Physics and Astronomy Department, Northwestern University, Evanston, Illinois 60208, U.S.A.

Correspondence to: m-olvera@northwestern.edu, bedzyk@northwestern.edu

1. Detailed Methods and Materials

1.1. DNA and DNA-coated-AuNP synthesis

DNA strands were synthesized using a MM48 DNA synthesizer (BioAutomation). The synthesis included a 3' propyl-thiol modification such that the gold-thiol chemistry could be used for DNA-AuNP attachment. Reagents from Glen Research were used. Synthesized strands included a 5'-AACAATTATACTCAGCAAAAAAAAAAAA-C_3SH-3' (sequence **A**) and a corresponding 18 base long complementary strand 5'-TTGCTGAGTATAATTGTT-3' (sequence **A'**). Due to their precedence for lacking off-target effects and promoting particle stability,[1] these DNA were utilized to prepare ds-DNA-AuNPs. For ss-DNA-AuNPs, the sequence 5'-T_{40}-C_3SH-3' was utilized. The choice of this unibase sequence avoided formation of any secondary structures.[2] All sequences were purified using reverse-phase high-performance liquid chromatography (RP-HPLC). The purity of the sequences was verified via a matrix-assisted laser desorption/ionization time-of-flight mass spectrometer (MALDI-TOF).

Au nanoparticles (AuNP) of nominal diameter 10 nm were purchased from TedPella. Thiol-modified oligonucleotides were tethered to the AuNP surface following previously established methods.[3] Briefly, 100 mM dithiothreitol (DTT, Sigma Aldrich) was used to reduce thiolated DNA strands for 1 hr, followed by DTT removal using a size-exclusion NAP5 column (GE Life Sciences). Thiolated DNA strands were added to a 1 mL of 0.01 nM AuNP solution at a ratio of 300 strands/AuNP. AuNP and DNA concentrations were calculated by applying Beer's law to UV-vis spectroscopy measurements (Cary 5000, Agilent) at 520 nm for AuNP and 260 nm for DNA. Sodium chloride (NaCl, Sigma Aldrich) was added slowly to the DNA/nanoparticle solution along with small amounts of 0.1 % sodium dodecyl sulfate (SDS, Sigma Aldrich) to ensure particle stability and to screen the electrostatic repulsion between

negatively charged DNA strands. The salting process was continued to reach a final NaCl concentration of 1 M to maximize DNA loading. The particles were then purified through three centrifugation cycles to remove excess DNA and NaCl from solution. Thereafter, these ss-DNA coated AuNP were suspended in deionized water. Prior to SAXS measurements, ss-DNA-AuNPs were combined with the appropriate salt solution (NaCl or $CaCl_2$, Sigma Aldrich) to a final nanoparticle concentration of 50 nM. For ds-DNA-AuNP formation, prior to salt addition, complementary strands (sequence **A'**) were added to solutions of AuNP functionalized with sequence **A** DNA. A ratio of 200 complements per nanoparticle was used to maximize the number of duplexes formed. To verify that the observations were not affected by excess of complementary DNA strands in the solution, additional experiments were performed by inducing ds-DNA-AuNP formation with 150, 100, or 50 complements/nanoparticle. No differences were observed for the four different concentrations of complementary DNA. Similar to ss-DNA-AuNP case, the final concentration of nanoparticles was 50 nM for the ds-DNA-AuNP. Subsequent to salt addition, all solutions were mixed by vortexing and allowed to equilibrate for at least 30 minutes prior to SAXS measurements.

To measure the number of duplexed strands per nanoparticle, ds-DNA-AuNPs were purified by centrifugation four times to remove excess complementary DNA from solution. The ds-DNA-AuNP nanoparticles were then suspended in 8M urea (Sigma Aldrich) at 45°C to cleave the duplex strand from its complementary thiolated strand, which was directly tethered to the AuNP. Centrifugation was used to separate the ss-DNA coated AuNP pellet from the released complementary strands in solution. A Quant-iT OliGreen (Invitrogen) assay was compared against a standard curve by measuring OliGreen fluorescence (λ_{ex} = 480 nm). The number of duplexed strands per particle was then calculated by dividing the DNA concentration in the

supernatant by the AuNP concentration, determined by UV-vis spectroscopy. For both ds-DNA-AuNPs and ss-DNA-AuNPs, the number of thiolated strands directly attached to AuNP was determined using a similar method. Here, the DNA strands were released by dissolving the AuNPs in 20 mM KCN at 50 °C before quantification through the OliGreen assay. For ss-DNA-AuNPs, the average number of DNA strands attached to a AuNP were found to be 65 ± 5 and 53 ± 4 for two separately prepared sample sets. For ds-DNA-AuNPs, the average number of thiolated strands (sequence **A**) per AuNP was 58 ± 2, and the number of duplexed strands was 23 ± 4.

1.2 X-ray measurements

SAXS experiments were carried out at beamline 5ID-D of the Advanced Photon Source. To avoid strong fluorescence from Au cores, X-ray energy was tuned to 10.0 keV (λ = 1.24 Å), which is below the *L* absorption edges for Au (11.9-14.3 keV). The X-ray spot size at the sample position was ~ 0.25 mm (H) × 0.25 mm (V), and the incident flux was ~ 10^{12} photons/s. The X-ray data was collected using three Rayonix CCD area detectors at ~ 0.2 m (range: q ~ 4.5 – 26 nm^{-1}), ~ 1.0 m (range: q ~ 0.8 – 4.6 nm^{-1}) and ~ 7.5 m (range: q ~ 0.015 – 0.9 nm^{-1}) from the sample. The liquid samples were placed in a 1.5 mm diameter quartz capillary tube embedded in a flow cell. The flow cell was in air. The flight paths between the three detectors were evacuated. To minimize radiation damage, the samples were continually flowing at a rate of 3 mm/s during data collection. All measurements were performed at room temperature.

For each DNA coated AuNP sample, five datasets were collected with an exposure time of 0.5 s each. To estimate background scattering, 5 sets of data for empty capillary and pure water were collected with 10s exposure, prior to each DNA-coated AuNP sample. To correct for fluctuations in the incident flux and the changes in X-ray transmission through different samples,

the incident and transmitted beam intensities were monitored using an ion chamber before the sample, and a pin-diode embedded in the beamstop placed before the SAXS detector (detector at ~7.5 m from the sample). X-ray polarization, transmission and detector solid angle corrections were applied to 2D data prior to azimuthal integration for obtaining 1D intensity profiles (using GSAS-II). The processed 1D data in Fig. 1 (main text) are the average of 5 sets that have been corrected for background scattering from empty capillary and pure water. The differences in scattering due to the different salt solutions were treated as parameters in the data fitting procedure (see, SAXS analysis section below).

Due to limited availability of beamtime at the synchrotron, additional measurements were performed on an in house Rigaku SMAXS-3000 set-up, which is equipped with a Cu microbeam anode and multilayer focusing mirrors. Characteristic X-rays with λ = 1.542 Å (CuKα) were selected. The X-ray spot size at the sample position was ~ 0.2 mm, and the incident flux was ~ 4×10^6 photons/s. The data was collected using a Vantec 2D multi-wire detector. The sample to detector distance (1.61 m) was calibrated using a silver behenate standard. The nanoparticle samples were placed in 1.5 mm quartz capillaries. The solutions were not flowing during these measurements. Data was collected with an exposure time of 25 minutes per sample. These experiments tested the reproducibility of the synchrotron measurements. The results from all the measurements are summarized in Tables S1-S2 below.

1.3. Molecular dynamics simulations

Coarse-grained molecular dynamics (MD) simulations were performed to calculate the effective interaction between two DNA-grafted nanoparticles immersed in aqueous electrolyte solutions. Two cases: ds-DNA-AuNPs in 5 mM and 50 mM $CaCl_2$ were studied. Our main goal was to quantify the mean force and the potential of mean force between these two DNA-grafted

nanoparticles in the absence of specific short-range interactions, i.e., only steric and Coulombic interactions were considered.

Water was taken as a continuum with dielectric permittivity ε = 78.5 at T = 298 K. The Bjerrum length is given by $l_b = e^2/4\pi\varepsilon_0\varepsilon k_B T$, where e is the proton charge, ε_0 is the vacuum permittivity and k_B is the Boltzmann constant. Ions were modeled as repulsive-core spheres of diameter 0.5 nm with point charges embedded in their centers. To reduce the simulation volume and the number of aqueous ions, AuNP was represented by a repulsive-core sphere of diameter 3 nm with 12 uncharged point-sites distributed on its surface. These point-sites refer to DNA attachment locations on the AuNP. The number of DNA/AuNP is consistent with the chosen AuNP size because for small AuNP ($R_{Au} \leq$ 10 nm), the maximum number of tethered DNA/AuNP can be approximated as $4\pi R_{Au}^{3/2}/2.19$.[4,5] The location of the 12 point-sites over the AuNP surface was determined by minimizing the potential energy of the sites assuming that they were interacting via a 1/r Coulombic potential. These point-sites were constrained to move only over the surface of the spherical nanoparticle core. Afterwards, all point-sites were uncharged and their relative position among them was rigidified. In order to have the same center of mass for the nanoparticle and the 12 uncharged rigid point-sites, the center of mass of the rigid sites was connected to the center of mass of the nanoparticle core by a very rigid spring with equilibrium length zero and spring constant 1,000,000 k_BT/σ, where σ = 0.5 nm. Even though the relative positions of the 12 uncharged point-sites on the surface of the nanoparticle were fixed, they were allowed to rotate freely with respect to the center of mass of the core-nanoparticle.

A single stranded DNA (ss-DNA) chain, approximating the A_{10} spacer in ds-DNA-AuNP, was modeled as a pearl-necklace polymer made of repulsive-core spheres (or beads). The diameter and valence of an ss-DNA repulsive-core sphere was 1 nm and -3, respectively. Four of

these ss-DNA repulsive-core spheres were connected linearly by rigid springs, yielding a total valence of -12 per ss-DNA chain. The centers of adjacent ss-DNA repulsive-core spheres were connected with each other by a rigid spring of equilibrium length 1 nm and a spring constant of 300 k_BT/σ, where σ = 0.5 nm. The linear charge density of an extended ss-DNA was 3 e^-/nm. The center of the first repulsive-core sphere of an ss-DNA chain was attached to one of the 12 sites lying on the surface of the uncharged nanoparticle via a rigid spring of equilibrium length 0.5 nm and spring constant 300 k_BT/σ. The last repulsive-core sphere of this pearl-necklace chain was attached to the first repulsive-core sphere of a double stranded DNA (ds-DNA) chain, which approximated the 18 base pair long ds-DNA segment in ds-DNA-AuNP. In this instance, the equilibrium length of the rigid spring connecting the center of last ss-DNA repulsive-core sphere and the center of the first ds-DNA repulsive-core sphere was 1.5 nm (the sum of their radii) with a spring constant of 300 k_BT/σ. A double stranded DNA (ds-DNA) chain was modeled as a rigid body constituted by five repulsive-core spheres of diameter 2 nm and valence -7.2. The centers of adjacent ds-DNA repulsive-core spheres were separated from each other by a distance of 1 nm. The total length of the ds-DNA rigid chain and the total valence were 6 nm and -36, corresponding to a linear charge density of 6 e^-/nm. The total valence of a chain constituted by an ss-DNA chain connected a ds-DNA chain was -48. The total valence of a neutral core-nanoparticle covered by 12 DNA chains was -576.

Consider the 6 different species of particles associated with the following repulsive-core spheres: 1) a neutral spherical core-nanoparticle of diameter 3 nm, 2) an uncharged point site on the surface of the spherical core-nanoparticle, 3) a spherical ss-DNA bead of diameter 1 nm, 4) a spherical ds-DNA bead of diameter 2 nm, 5) a divalent spherical cation of diameter 0.5 nm, and 6) a spherical monovalent anion of diameter 0.5 nm. The pair interaction between a particle of

species *i* and a particle of species *j* separated at a distance *r* is given by

$$\beta u_{ij}(r) = \beta u_{ij}^{rc}(r) + \frac{l_b}{r} q_i q_j \qquad \text{(S1)}.$$

Here, $\beta = 1/(k_B T)$. The repulsive-core (*rc*) interaction potential is modeled as follows: a hard core potential $\beta u_{ij}^{rc} = \infty$ for $r \le \Delta_{ij}$, and a shifted-truncated Lennard Jones potential

$$\beta u_{ij}^{rc} = 4[(\frac{\sigma}{r - \Delta_{ij}})^{12} - (\frac{\sigma}{r - \Delta_{ij}})^{6}] + 1 \qquad \text{(S2)}$$

for $\Delta_{ij} < r < \Delta_{ij} + 2^{1/6}\sigma$, and $\beta u_{ij}^{rc} = 0$ for $r \ge \Delta_{ij} + 2^{1/6}\sigma$. The parameter $\Delta_{ij} = (d_i + d_j)/2 - \sigma$ then acts as the hard-core diameter in this interaction, where d_i and d_j are the repulsive-core sphere diameters for species *i* and *j*, defined above, and σ regulates the hardness of interactions among all particles. In this way, $\beta u_{ij}^{rc}(\frac{d_i + d_j}{2}) = 1$ for all particles with non-zero radius, and the form of the potential guarantees a soft continuous repulsion beyond the inner core, that is, for $r > \Delta_{ij}$. Here, we set $\sigma = 0.5$ nm, which is the diameter of the ions.

Two identical DNA-grafted nanoparticles were placed at symmetric fixed positions along one of the body diagonals of a cubic simulation box. As described above, the uncharged point-sites over the surface the core-nanoparticles were free to rotate as a rigid body around the center of mass of the core-nanoparticles. Mobile ions surrounded both nanoparticles inside a cubic simulation box under periodic boundary conditions. The total amount of ions was such that the whole system was electroneutral for a given salt concentration. Molecular Dynamics (MD) simulations were performed using the LAMMPS package[6] (available at http://lammps.sandia.gov) in the NVT ensemble via a Nosé–Hoover thermostat[7,8] at a renormalized temperature $T' = k_B T / \varepsilon = 1$. The time step used was 0.001τ, where τ is the

associated reduced Lennard-Jones unit of time defined in terms of the mass and diameter of the ions. For the highest electrolyte concentration, the total number of ions used in the simulations was around 5000. The mean force exerted over one DNA-grafted nanoparticle is defined as the total time averaged force acting over this DNA-grafted nanoparticle due to the repulsive-core and Coulombic interactions with the other DNA-grafted nanoparticle (whose center of mass is located at a fixed distance) and the surrounding ions. 10 million MD time steps were used to thermalize the system. The total repulsive-core and electrostatic forces acting over each DNA-grafted nanoparticle were sampled each 10 MD time steps (in a compromise between efficiency and reduction of time correlations), and between 40 and 80 millions of MD time steps were performed to calculate the time averaged forces. Converged mean forces displayed the same magnitude but opposite direction as it was expected by the symmetry of the whole system. Several mean forces were calculated for different separation distances between the center of masses of the DNA-grafted nanoparticles. The potential of mean force was then calculated integrating the mean forces as a function of the separation distances starting at a position where the mean force is approximately zero. Thus, the potential of mean force represents the required work to bring one DNA-grafted nanoparticle from a distant position in the bulk electrolyte up to a certain distance close to the other DNA-grafted nanoparticle.

Due to the necessity of sampling large number of orientations and configurations for the DNA-coated nanoparticles in the explicit presence of all the electrolyte ions, the above described calculations for ds-DNA-AuNP in $CaCl_2$ solutions took 1-2 months for each point on the potential of mean force curve, while using several dozen of the fastest intel processors. A much longer computational time (at least 6-8 months, with a few hundred of dedicated processors) is expected for the case of DNA-coated AuNPs in NaCl solutions because of the 10 fold increase in

the number of electrolyte ions at the onset of crystallizations (750 mM NaCl vs 50 mM $CaCl_2$). Therefore, we did not perform these calculations. However, we note that our previous MD simulation and liquid state theory study[9] shows that 1:1 electrolytes (*eg.* NaCl) at high concentrations (*eg.* 1M) can induce attractions between like charged spherical colloids.

1.4. Monte-Carlo Simulations

Canonical Monte Carlo simulations of a dense system of hard spheres (random close-packed spheres) were performed in a cubic simulation box with periodic boundary conditions.[10,11]According to the classical Metropolis algorithm,[10,11] small displacements of the hard spheres were accepted in the absence of overlaps. As usual, the volume fraction (ϕ_s = 0.634) was defined as the ratio of the volume of the hard spheres and the simulation box volume. The algorithm by Clarke and Wiley was used[12] to generate an initial configuration. Very small acceptance ratios, 0.01 or below, were used to adjust the maximum displacement of 1000 non-overlapping hard spheres. 10 million attempted moves per particle, or Monte Carlo cycles, were performed initially and then discarded. 30 million additional Monte Carlo cycles were used to calculate the canonical average of the hard sphere density profiles.

2. SAXS analysis

2.1. Scattered intensity from isolated DNA coated AuNPs

The scattered intensity from DNA-coated AuNPs is largely due to the electron-dense Au cores. Therefore, for simplicity, we ignore the associated DNAs and the aqueous ions. Under this approximation, the scattered intensity $P(q)$ from DNA-coated AuNPs in the isotropic gas phase is calculated as

$$P(q) = A \times \left\langle \left| F(q, R_{Au}) \right|^2 \right\rangle_{R_{Au}} + bkg \qquad \text{(S3).}$$

Here, $F(q, R_{Au})$ is the q-dependent form factor for an isolated AuNP of radius R_{Au}, *i.e.*, the scattering amplitude due to the interference of X-rays scattered from different portions of the same AuNP.

$$F(q, R_{Au}) = V_{Au} \times (\rho_{Au} - \rho_{wat}) \times [\sin(qR_{Au}) - (qR_{Au}) \times \cos(qR_{Au})]/(qR_{Au})^3 \qquad \text{(S4).}$$

Here, V_{Au} and ρ_{Au} (= 4660 e/nm^3) are the volume and electron density of the Au core, and ρ_{wat} (= 334 e/nm^3) is electron density of water. To take into account polydispersity of Au cores, the intensity from an isolated AuNP ($\left| F(q, R_{Au}) \right|^2$) is averaged over a Schulz distribution[13] [Pr(R_{Au})] for Au core sizes.

$$\Pr(R_{Au}) = \left[\frac{z+1}{\langle R_{Au} \rangle}\right]^{z+1} \frac{R_{Au}{}^{z}}{\Gamma(z+1)} e^{\left[-(z+1)\frac{R_{Au}}{\langle R_{Au} \rangle}\right]} \qquad \text{(S5).}$$

$\langle R_{Au} \rangle$ is the mean radius for the Au cores, $\Gamma(z+1)$ is the gamma function, and the percent polydispersity is given by $\frac{100}{\sqrt{z+1}} = \frac{100 \times \sqrt{\Sigma^2}}{\langle R_{Au} \rangle}$, where Σ^2 is the variance of the distribution. For cases where no aggregation of DNA-coated AuNPs is observed, the empty capillary and the water background subtracted SAXS intensity is fitted with equation S3. The fitting parameters are $\langle R_{Au} \rangle$, z, and the two constants A and bkg. The constant A is directly proportional to the number density of nanoparticles in the solution, the scaling factor for converting the intensity to absolute scale, and the changes in electron density contrast because of changes in salt concentration. The constant bkg is only affected by the scattering from the aqueous ions; bkg increases with increasing salt concentration.

2.2. Structure factor for crystalline lattices

The structure factor $S(q) = I(q)/P(q)$ arises due to the interference between X-rays scattered from distinct spatially correlated nanoparticles. Here, $I(q)$ is the background subtracted measured scattered intensity and $P(q)$ is defined above in Eq. S3. For an aggregate exhibiting crystalline ordering, $S(q)$ can be written under the "decoupling approximation"[14] as

$$S(q) = [1 + \beta(q)(Z(q) - 1)G(q)] \quad \text{(S6)}.$$

As seen from Eq. S6, $S(q)$ is comprised of three functions: $Z(q)$, which reflects the symmetry of the crystal lattice, $\beta(q)$ arises due to the presence of nanoparticles of different sizes within a given crystalline domain and $G(q)$, captures the lattice disorder due to the displacements of nanoparticles about their mean positions, respectively. These three functions are defined below.

$$Z(q) = \frac{1}{q^2} \sum_{\{hkl\}} m_{hkl} \left| \sum_j e^{i2\pi(hx_j + ky_j + lz_j)} \right|^2 L_{hkl}(q) \quad \text{(S7)}$$

$$\beta(q) = \frac{\left\langle F(q, R_{Au}) \right\rangle^2}{\left\langle F(q, R_{Au})^2 \right\rangle} \quad \text{(S8)}$$

$$G(q) = e^{-\sigma^2 d_{NN}^2 q^2} \quad \text{(S9)}.$$

In the definition for $Z(q)$, the outer sum extends over sets of symmetry-equivalent $\{h\ k\ l\}$ reflections with m_{hkl} being the multiplicity or the number of elements in each set. The inner sum extends over all the j particles in the unit cell with each particle center located at a fractional coordinate position (x_j, y_j, z_j). L_{hkl} is the line shape for a given $\{h\ k\ l\}$ reflection. In our analysis, we have used Lorentzians, with identical widths for the profiles describing the different $\{h\ k\ l\}$ reflections. In the definition for $G(q)$, σ parametrizes the relative variations of the particle positions about their lattice sites and d_{NN} is the mean distance between the nearest-neighbor

particles in the crystal. In our fits for FCC structure factors (Fig. 2A, main text), the best fit σ ranged between 0.03 and 0.05.

2.3. Radial distribution function

The radial distribution function is defined as the Fourier transform of the renormalized structure factor [$S(q)$-1].[13] Specifically,

$$g(r) = [\rho(r) - \rho_0] = \frac{1}{2\pi^2 r}\int_0^\infty q[S(q) - 1]\sin(qr)dq \qquad \text{(S10)}.$$

Here, $\rho(r)$ is the number density of DNA functionalized AuNPs as a function of radial distance r from the center of any given nanoparticle, and ρ_0 is the average number density in an aggregate.

3. Samples examined by SAXS

The datasets discussed in the main text are summarized in Table S1. To test the reproducibility of these measurements, additional SAXS experiments were carried out for ss-DNA-AuNP in NaCl and $CaCl_2$ solutions. For ss-DNA-AuNP in NaCl, three ionic strengths were tested for two separately prepared sample sets: 30 mM and 1500 mM (trial 1) and 1500 mM and 2500 mM (trial 2). Aggregation of nanoparticles was not observed in any of the cases. The data from trial 1 is shown in Fig. 1A (main text). For this case, the number of DNA on the AuNP was not measured. For trial 2, the number of DNA on AuNP was 65 ± 5. For ss-DNA-AuNP in $CaCl_2$, three separately prepared sample sets were used. These are summarized in Table S2. The data from Trial 2 is the same as in Table S1. As can be seen from Table S2, for a given ionic strength μ_s, the nearest neighbor distance d_{NN} varies by ~ 10% in different datasets. For example at μ_s = 1500 mM, d_{NN} = 21.5, 19.4 and 20.0 nm are observed in three different trials. The only experimental control parameter that is variable in these studies is the number density of the DNA.

Further systematic studies with greater control over the DNA coverage are required to quantitatively describe the dependency of the d_{NN} on the number of DNA on the AuNP. Nevertheless, these experiments validate the qualitative argument that the packing of AuNPs undergoes gas to FCC to glass-like rearrangements as the ionic strength is increased. Specifically, for ss-DNA-AuNP in $CaCl_2$, the FCC lattice is observed only in a narrow range of μ_s ~ 1050-1500 mM.

System	μ_s (mM)	Packing	d_{NN} (nm)
ss-DNA-AuNP/$CaCl_2$	150	Gas-like	N/A
	450	Gas-like	N/A
	750	Gas-like	N/A
	900	Gas-like	N/A
	1050	FCC	20.6
	1350	FCC	19.9
	1500	Glass-like	19.4
	1650	Glass-like	19.2
	1950	Glass-like	19.2
ds-DNA-AuNP/NaCl	30	Gas-like	N/A
	150	Gas-like	N/A
	300	Gas-like	N/A
	750	FCC	26.0
	1500	Glass-like	24.8
ds-DNA-AuNP/$CaCl_2$	30	Gas-like	N/A
	150	FCC	24.3
	300	Glass-like	23.1
	750	Glass-like	23.0
	1500	Glass-like	22.7

Table S1. Summary of samples discussed in the main text. Note, for FCC lattices $d_{NN} = a_{FCC}/\sqrt{2}$. For glass-like assemblies d_{NN} is obtained from the position of the first peak in $g(r)$. The data was collected at beamline 5ID-D of the Advanced Photon Source.

System	Trial #	DNA/AuNP	μ_s (mM)	Packing	d_{NN} (nm)
ss-DNA-AuNP/$CaCl_2$	1	Not measured	30	Gas-like	N/A
			150	Gas-like	N/A
			300	Gas-like	N/A
			750	Gas-like	N/A
			1500	FCC	21.5
	2	65	150	Gas-like	N/A
			450	Gas-like	N/A
			750	Gas-like	N/A
			900	Gas-like	N/A
			1050	FCC	20.6
			1350	FCC	19.9
			1500	Glass-like	19.4
			1650	Glass-like	19.2
			1950	Glass-like	19.2
	3	53	600	Gas-like	N/A
			1200	FCC	20.4
			1500	FCC	20.0
			1950	Glass-like	18.9
			2400	Glass-like	18.8

Table S2. Summary of observations for ss-DNA-AuNP in $CaCl_2$ solutions from three separately prepared sample sets. The data from Trial 1 and Trial 2 were collected at beamline 5ID-D of the Advanced Photon Source. The data from trial 3 was collected in the Northwestern University X-ray diffraction facility.

4. Dynamic light scattering measurements

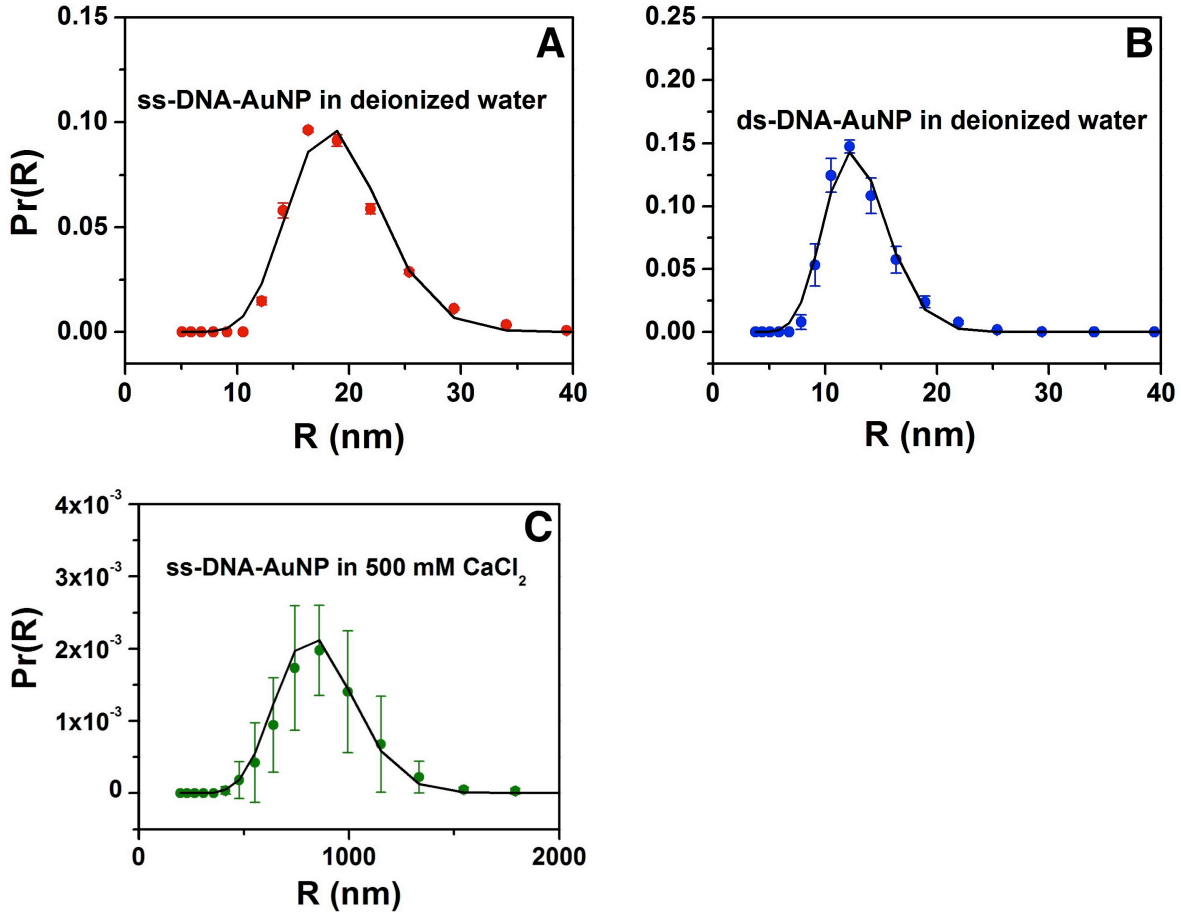

Figure S1. Dynamic light scattering (DLS) measurements of DNA coated AuNPs and their assemblies. DLS-derived probability distribution [$Pr(R)$] for the hydrodynamic radius (R) of (**A)** ss-DNA-AuNP in pure water, (**B)** ds-DNA-AuNP in pure water and (**C)** aggregates of ss-DNA-AuNP in 500 mM $CaCl_2$. The data shown is the average of 3 measurements, with the error bars representing the standard deviation. The black lines are fits based on Schulz distribution for R. The data was collected on a Malvern Zetasizer Nano ZS system (λ = 633 nm laser).

As described in section 2 above, the SAXS intensity is largely dominated by scattering from the Au cores. Therefore, for DNA coated AuNPs, the radial extent of the DNA shell cannot be readily extracted from the SAXS data. In order to gain insight into the overall size of the DNA-coated-nanoparticles, we performed dynamic light scattering (DLS) studies on ss-DNA-AuNP and ds-DNA-AuNP dispersed in pure water. Fig. S1A-B show that the mean radius (R) of ss-DNA-AuNP and ds-DNA-AuNP in pure water is R =19.2 and R = 13.0 nm. These R in salt-free solutions should correspond to the maximum radii for these DNA coated nanoparticles because

with increasing salt concentration, the radial extension is expected to decrease for the single stranded DNA segments present on both the ss-DNA-AuNP and the ds-DNA-AuNP.[2] Therefore, these DLS-derived R were used to estimate the upper bounds for the volume fraction of these nanoparticles (main text).

In salt free conditions, the DLS-derived radius of ss-DNA-AuNP is ~ 48% higher than the radius of ds-DNA-AuNP. By contrast, in 500 mM $CaCl_2$, the SAXS-derived nearest-neighbor distance d_{NN} = 19.4 nm and 22.7 nm in ss-DNA-AuNP and ds-DNA-AuNP aggregates (table S1). Assuming tangential contact between nanoparticles, *i.e.* $d_{NN}/2 = R$, the radius of ss-DNA-AuNP becomes ~ 14% smaller than the radius for ds-DNA-AuNP in 500 mM $CaCl_2$. These combined SAXS-DLS observations are consistent with the architecture of the DNA strands used and the expected response of these DNA strands to the salt environment, as described below.

Recall, that the DNA strand on ss-DNA is a 40 base long poly-T sequence (T_{40}), and the DNA strand on ds-DNA consists of a 28 base long ss-DNA, with 18 bases farthest from the Au surface duplexed with a complementary DNA. In zero-salt condition, where the electrostatic repulsions between the negative charges along the DNA strand are very weakly screened, the flexible ss-DNA strands are expected to be stretched, resulting in a larger radial extension for the ss-DNA-AuNP, where the DNA coating has a longer base sequence (T_{40}). With increasing salt concentration, the radial extension is expected to reduce drastically for the ss-DNA,[15] but not for the rigid rod-like duplexed segment (on ds-DNA-AuNP) because of the large persistence length (L_p ~ 50 nm) for ds-DNA.[16] Therefore, at high salt concentrations, the R for the ds-DNA-AuNP is higher that for the ss-DNA-AuNP.

In order to gain information regarding the size of the aggregates of DNA-coated nanoparticles, DLS measurements were performed for ss-DNA-AuNP in 500 mM $CaCl_2$.

Depending on the sample used (different trials), the mean R of the aggregates was found to vary between ~ 700 -1000 nm. The average size distribution obtained from 3 different measurements is shown in Fig. S1C, which shows a mean R = 860 nm. The large error bars are a result of the aforementioned variations in the size distributions observed in different trials.

5. Comparison between experimental nearest neighbor distances and theoretical estimates

Here, we provide evidence that in the observed assemblies, the DNA-coated nanoparticles are packed tightly. Tables S1-S2 and Figs. S2A-S2B show that the nearest neighbor distances (d_{NN}) decrease with increasing μ_s to reach a near constant value in the glassy state. To gain some insight into the packing of nanoparticles, it is necessary to estimate the radial extent of the DNA corona as a function of μ_s. Previous studies on the assembly of ss-DNA coated AuNPs via Watson-Crick hybridization in bulk solutions[17] or via 2D confinement and ion-mediated attractions at a liquid/vapor interface[2] show that the radial extent t_{DNA} of ss-DNA tethered to spherical AuNPs can be estimated using the Daoud-Cotton model or its modifications [modified Daoud-Cotton Model (mDC)]. These models take into account the curvature of the AuNP, the number density of the tethered DNA and the effect of the salt concentration. Following Tan *et. al.*,[2]

$$t_{DNA} = R_{Au}[1 + \frac{KNb}{R_{Au}}(S\mu_s^{-\eta})^{1/3}]^{3/5} - R_{Au} \qquad \text{(S11)}.$$

Here, N is the number of bases in the ss-DNA strand, b = 0.65 nm is the inter-base separation along the DNA contour, S is the surface number density of the DNA tethered to AuNP of radius R_{Au}, and K and η are constants of the order unity. In particular, for 2D hexagonally packed arrays of ss-DNA coated AuNPs at the liquid/vapor interface, the observed d_{NN} [assumed to be equal to

the hydrodynamic diameter for the nanoparticle (Fig. S2C)] could be successfully described by the mDC parameters (K, η) = (1.4, 1) and (K, η) = (2.1, 1) for the cases of assemblies in the presence of $MgCl_2$ and NaCl, respectively. Similarly, in FCC crystals of ds-DNA coated spherical AuNPs via Watson-Crick hybridization in bulk solutions, it was observed that the radial extent of the ds-DNA corresponds to a ~ 0.26 nm rise/base-pair.[18]

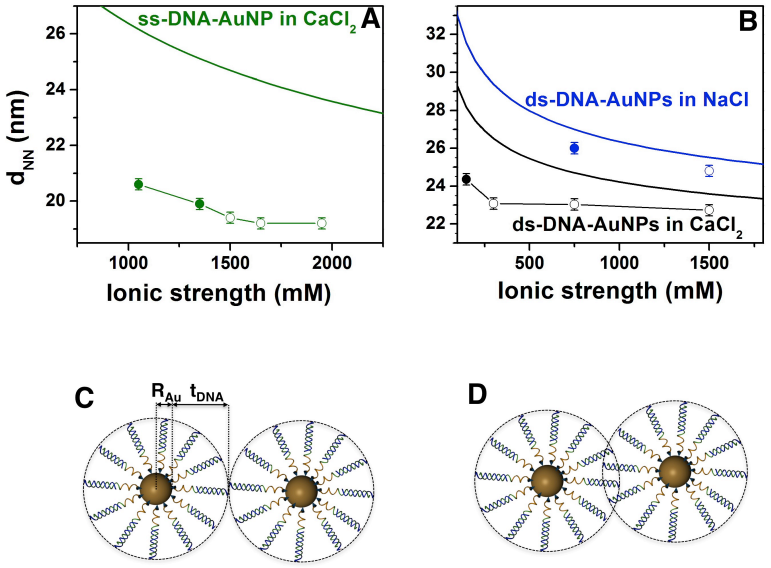

Figure S2. SAXS-derived nearest neighbor distances in assemblies of DNA coated AuNPs. Nearest-neighbor distance (d_{NN}) as a function of solution ionic strength. (**A**) ss-DNA-AuNP in $CaCl_2$ and (**B**) ds-DNA-AuNP in NaCl (blue) and $CaCl_2$ (black). Filled circles correspond to FCC lattices and open circles correspond to glassy assemblies. Solid lines connecting the data points are guide to the eye. Solid curves are estimates for the diameter ($2R$) of the DNA-grafted-AuNPs that are based on the parameters from references 2 and 18. The plotted data is from Table S1. Schematic for DNA-grafted nanoparticles in tangential contact (**C**) and in interdigitated configuration (**D**).

Figures S2A-B show the estimates for the hydrodynamic diameter ($2R$) of DNA-coated nanoparticles (solid lines) that are based on the combination of the above described ss-DNA and ds-DNA parameters. Figs. S2A-B show the calculated $2R$ are larger than the observed d_{NN} by as much as ~ 25%. There are two possibilities for these differences. First, the aforementioned mDC parameters[2] are overestimated because the 2D confinement of nanopaticles in that study could have induced assembly even in a regime where the interparticle center to center separation was larger than $2R$. This hypothesis is partly supported by the observation that a closer match to the

observed d_{NN} in the present study is obtained with slightly reduced value of the parameter K: (K, η) = (1.8, 1) and (K, η) = (0.8, 1) for the cases of aggregates in NaCl and $CaCl_2$ (Fig. S3). Second, it is possible that in the electrolyte-mediated assembly (present study), the DNA chains on neighboring nanoparticles interdigitate (Fig. S2D). It should be noted however, that a large region of overlap between DNA coronas on neighboring particles is prohibitive due to the ensuing steric repulsions between DNA chains, as suggested by our MD simulations (Fig. 3, main text). In the MD simulations, the minimum in the interparticle interaction potential occurs at an interparticle separation where the DNA coronas are, roughly speaking, just touching. Overall, the above observations suggest that DNA coated AuNPs are packed tightly without strong overlap between the DNA coronas on neighboring AuNPs.

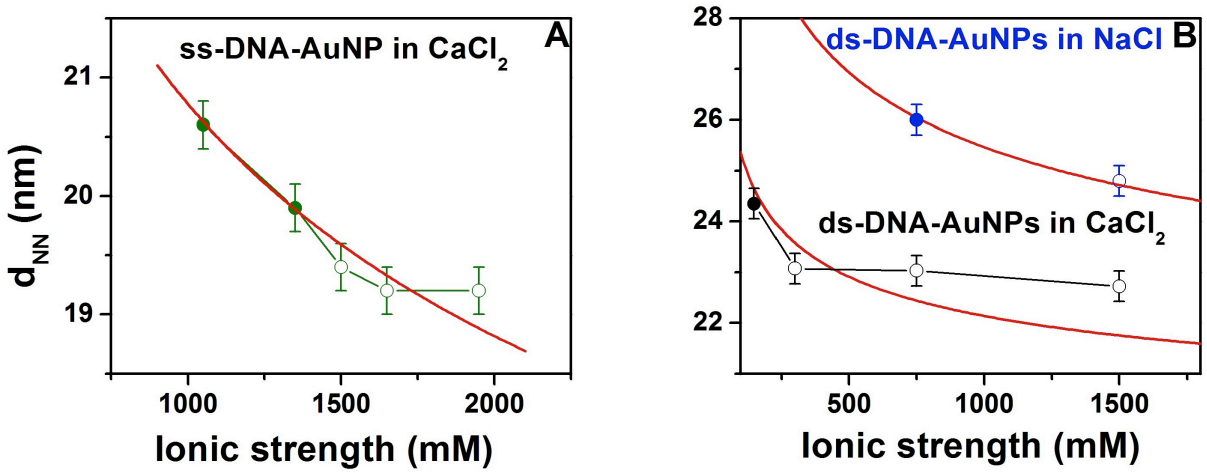

Figure S3. Nearest-neighbor distance (d_{NN}) as a function of solution ionic strength. (**A**) ss-DNA-AuNP in $CaCl_2$ and (**B**) ds-DNA-AuNP in NaCl (blue) and $CaCl_2$ (black). Filled circles correspond to FCC lattices and open circles correspond to glassy assemblies. Solid lines connecting the data points are guides to the eyes. Solid red curves are estimates for the hydrodynamic diameter of the DNA-grafted-AuNPs that are based on the modified mDC parameters described above. The plotted data is from Table S1.

6. Ion correlations in the presence of DNA-grafted nanoparticles

To understand the role of ions in mediating the assembly, it is important to analyze the inter-ionic and the ion-nanoparticle positional correlations. Figure S4 shows the MD-derived average density profiles of monovalent anions surrounding the divalent cations for the cases of μ_s = 15 mM (Fig. S4A) and 150 mM (Fig. S4B). The calculations are for the case when the two identical ds-DNA-capped nanoparticles are placed along one of the body diagonals of a cubic simulation box. Here and hereinafter, the length of the cubic simulation box for both salt concentrations is 34 nm, and both ds-DNA-capped nanoparticles are located at symmetric fixed positions with respect to the center of the simulation box. The separation between the centers of mass of the two nanoparticles is 20.45 nm. At this separation, the interparticle interactions are weakly repulsive for μ_s = 15 mM and weakly attractive for μ_s = 150 mM (Fig. 3, main text). The two nanoparticles were allowed to rotate freely about their center of mass. Fig. S4 shows that for anion-cation separation equal to the ionic diameter (contact distance), the local concentration of monovalent

anions is enhanced with increasing μ_s. A depletion region of monovalent ions is also observed closer to the surface of divalent cations.

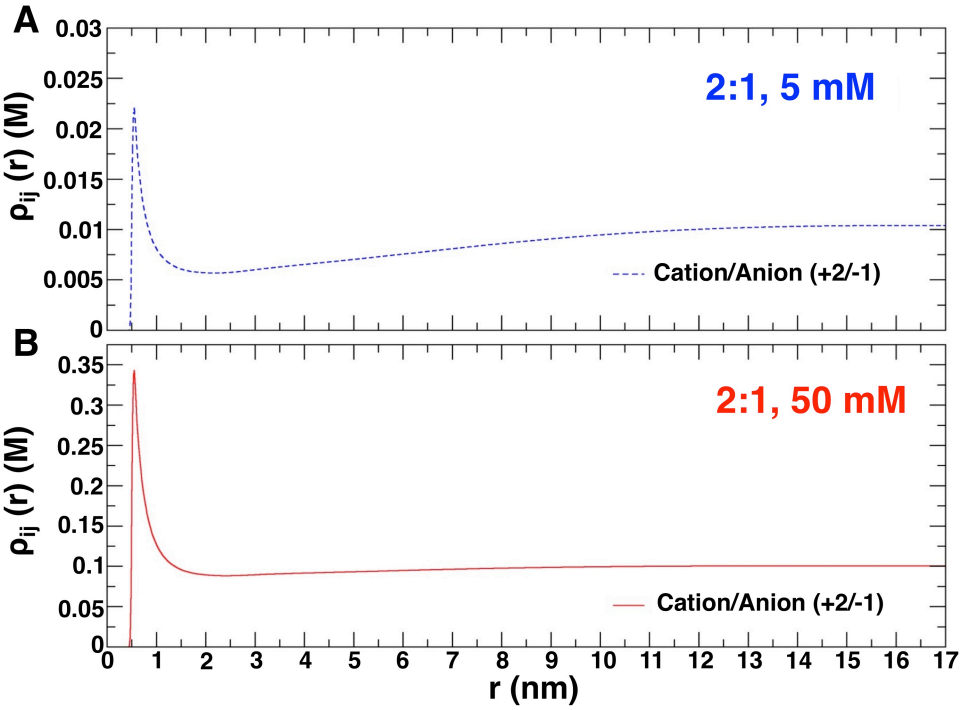

Figure S4. Average density profile of monovalent anions surrounding divalent cations in the presence of two ds-DNA-coated AuNPs. Two concentration cases were examined for this 2:1 electrolyte (**A**) 5 mM (μ_s = 15 mM) and (**B**) 50 mM (μ_s = 150 mM).

The above described density profiles can be interpreted in terms of the potential of mean force as a function of the separation between monovalent anions and divalent cations (Fig. S5). Fig. S5A shows an attractive interaction between monovalent and divalent ions at low solution ionic strength (μ_s = 15 mM). The maximum strength of this attraction occurs when the centers of the cation and the anion are located at a separation of one ionic diameter approximately. At larger separations, this attractive interaction decreases and a repulsive barrier is observed. When the concentration of the salt is increased ten times (Fig. S5B), the maximum depth of the attractive well is nearly doubled, and the repulsive barrier almost vanishes. Thus, the ion pairing

under such conditions is greatly facilitated as compared to the lower concentration case displayed in Fig. S5A.

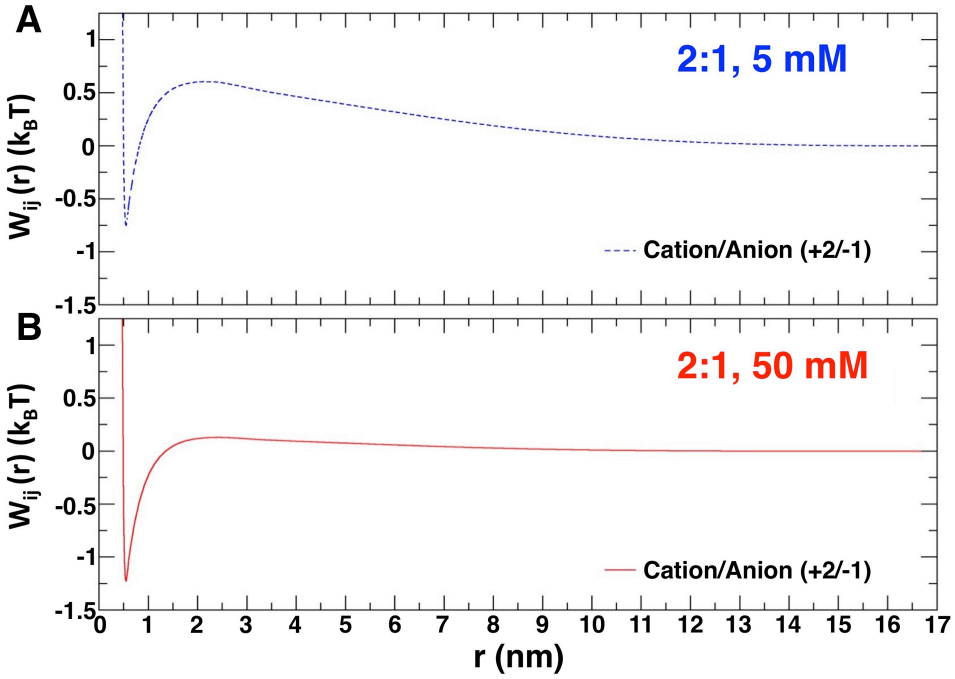

Figure S5. Potential of mean force between the divalent cation and the monovalent anion as a function of inter-ion separation. Two concentration cases were examined for this 2:1 electrolyte (**A**) 5 mM (μ_s = 15 mM) and (**B**) 50 mM (μ_s = 150 mM)

The effect of the ionic strength on the spatial correlations between the ds-DNA capped nanoparticles and the surrounding divalent counterions is analyzed in Fig. S6. The average density profiles for divalent cations surrounding a DNA-grafted nanoparticle is displayed for two salt concentrations: 5 mM (Fig. S6A) and 50 mM (Fig. S6B). These figures show that as the ionic strength is increased, the local concentration of the divalent cations also increases. This enhancement is particularly evident for regions very close to and far away from the neutral-core-surface of the DNA-grafted nanoparticle.

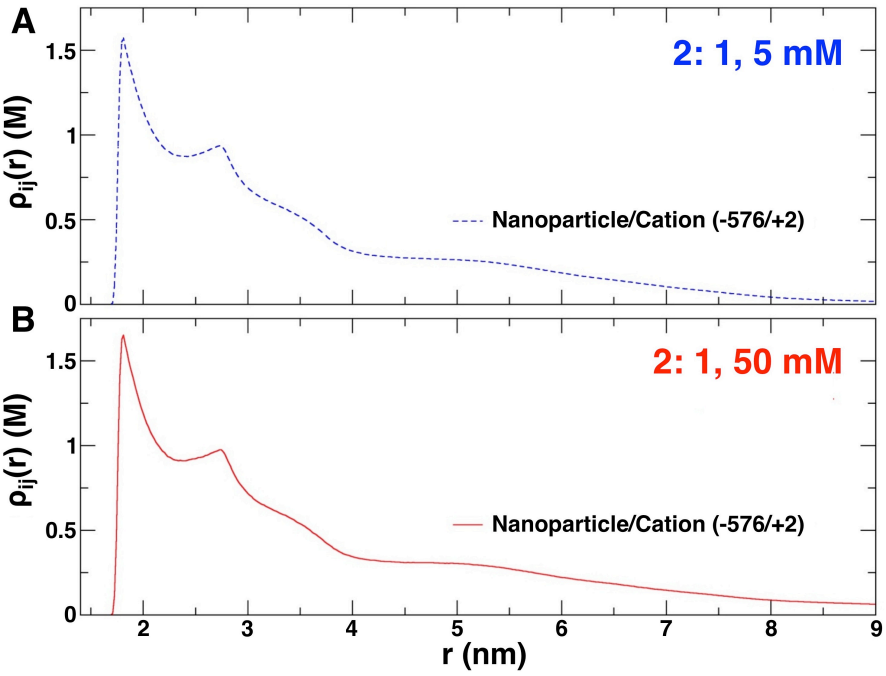

Figure S6. Average density profiles of divalent cations surrounding a single dsDNA-grafted nanoparticle. In (**A**) the salt concentration of the 2:1 electrolyte is 5 mM (blue dashed line), and in (**B**) the salt concentration of the 2:1 electrolyte is 50 mM (red solid line). Here, 'r' represents the distance from the surface of the nanoparticle core.

In order to quantify the neutralization of DNA-grafted nanoparticles charge by the electrolyte, we have calculated the average number of divalent cations and monovalent anions associated to a DNA-grafted nanoparticle when the two DNA-grafted nanoparticles are located at symmetric fixed position with respect to the center of the simulation box. The center-to-center interparticle separation here too was 20.45 nm. The number of ions associated with a single DNA-grafted nanoparticle is defined as the number of ions enclosed by a sphere of diameter 17.6 nm, with the center of this sphere matching the center of mass of the nanoparticle. On average, it was observed that there were 280 cations and 10 anions associated with a single ds-DNA-grafted nanoparticle, when the salt concentration was 5 mM. When the concentration of the electrolyte was 50 mM, an average of 349 cations and 134 anions were associated with a single ds-DNA-grafted nanoparticle. As the valence of a single ds-DNA-grafted nanoparticle is -576, the above calculations suggest that the charge of a single DNA-grafted nanoparticle is neutralized 95% and

98% by a divalent salt at ionic concentrations of 5 mM and 50 mM, respectively. These observations are consistent with previous DFT calculations and SAXS experiments for ion distribution surrounding a ds-DNA-grafted nanoparticle in the presence of monovalent ions with different ionic sizes.[4] The average number of triplets, which are the smallest ion pairs associated with a single DNA-grafted nanoparticle, can be also estimated from the average number of monovalent anions previously calculated. We estimate that a single DNA-grafted nanoparticle has 5 and 67 associated triplets for 5 mM and 50 mM salt concentration, respectively.

All the features discussed above suggest an enhancement of the average long-ranged electrostatic cohesive energy between divalent cations and monovalent anions at high ionic strengths in the presence of highly charged DNA-grafted nanoparticles.

7. Like-charge attractions

Like-charge attractions appear in simple bulk electrolytes under a wide range of conditions. Positive ions attract negative ions that in turn attract other positive ions, which could result in a mean attractive force between two positive ions (mediated by negative ions). Whether this mean attraction is significant or present at all, depends strongly on the ion density and electrostatic coupling strength. To investigate the relevance of this effect, we evaluate the radial distribution functions of primitive model electrolytes, for parameters that correspond to aqueous solutions of $CaCl_2$ and NaCl, and show results in Fig. S7. The black curves are solutions of the Ornstein-Zernike equation with a DHEMSA closure[19] and the red curves follow from a mean field theory (Poisson-Boltzmann). A comparison between the two methods reveals that the mean field results underestimate the typical range of $g(r)$ and miss typical density oscillations that result from charge ordering and cluster formation (ionic correlations). The Debye length, which follows as a

natural decay parameter in Poisson-Boltzmann theory, is therefore not an exact measure for the electrostatic correlation length at higher ion concentrations. Instead, the ionic correlations typically extend over several nanometers, even at higher concentrations where the Debye length is of the order of a few Å. Figure S7 shows that every ion influences its environment over about 2.5 nanometers under the given conditions, and that a local excess of like-charge is present within that environment. The hydrated ion radii used in these calculations are: 3.58 Å for Na^+, 3.32 Å for Cl^-, and 4.12 Å for Ca^{2+}.[20]

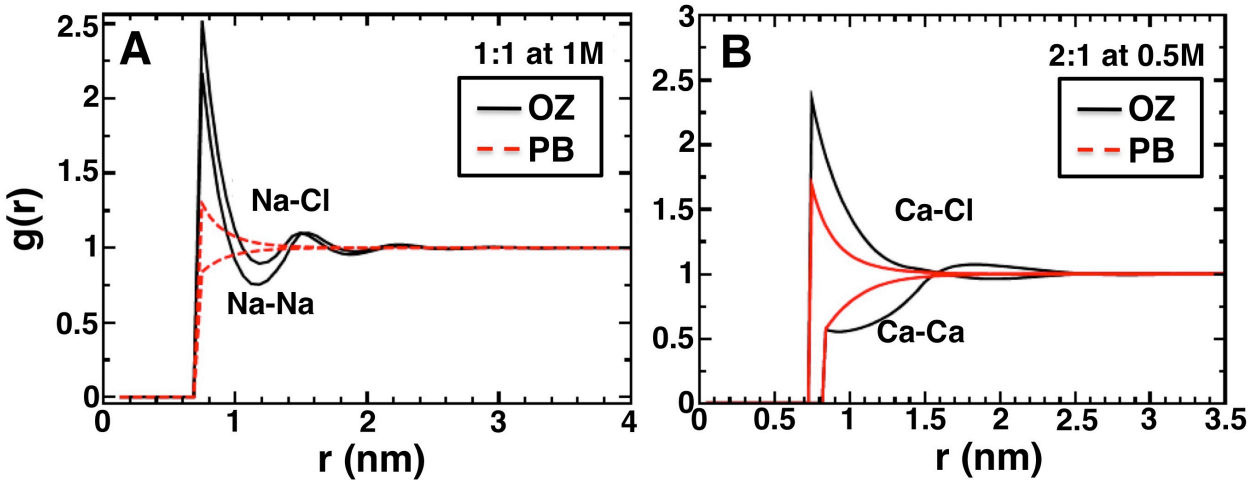

Figure S7. Radial distribution functions between two like charges [Na-Na (**A**); Ca-Ca (**B**)] and two opposite charges [Na-Cl (**A**) Ca-Cl (**B**)]. Comparison is shown between an almost exact method (OZ, black curves) and a mean field method (PB, red curves). The OZ results show oscillations that the PB results miss, and the range of the $g(r)$ is longer than expected by PB theory.

From the radial distribution functions we obtain the mean forces directly via Boltzmann's distribution: $U_{mean}(r) = -k_B T \ln[g(r)]$, and show the results in Fig. S8. The mean force between two opposite charges is rather weak, and between two like charges even weaker (< 1 $k_B T$), but the effects are cumulative when one considers the mean forces between two highly polyvalent nanoparticles that offer many charged surface groups. The local environment of a DNA-grafted nanoparticle may contain up to thousands of ions[4] such that tiny changes in the free energy per ion may add up to a significant change in the free energy per nanoparticle. The next section

describes the effective forces that result from the overlap of two 'regions of influence' exerted by two nanoparticles.

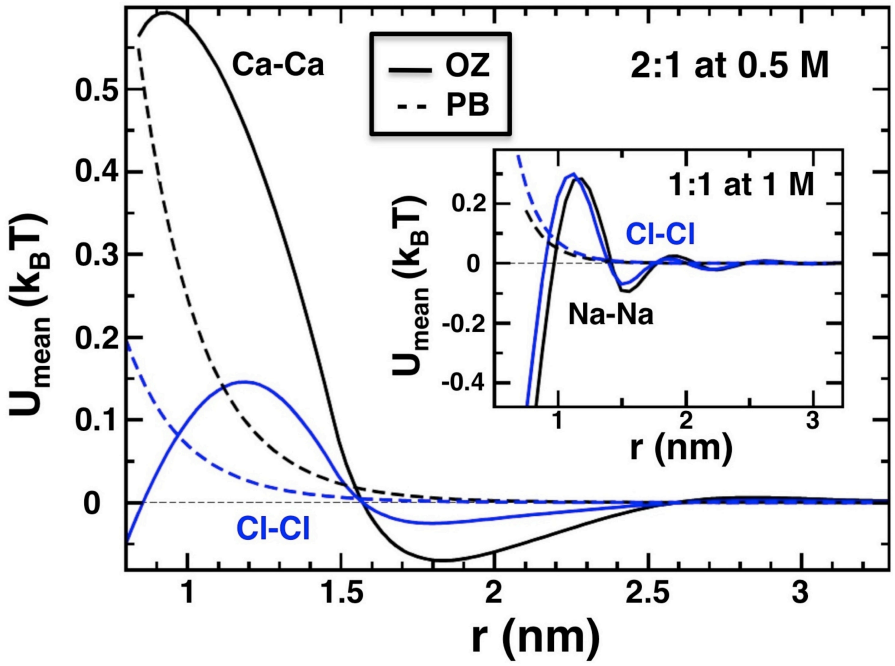

Figure S8. Mean potentials between the ions in a 2:1 electrolyte and a 1:1 electrolyte (inset), corresponding to the data in Fig. S7. The potential between Ca and other Ca ions (black), and between Cl ions (blue) shows an attractive well. The mean field data (dashed lines) miss these attractions. Weak as the attraction may be, it may add up to strong interactions between polyvalent macroions.

Moving to the next level of complexity, we calculate the ion-induced force between two parallel boundaries that are smooth, structureless, homogeneously charged, and dielectric. We use a liquid-state method for anisotropic systems, based on the Ornstein-Zernike equation with anisotropic hypernetted chain (AHNC) closure,[21-23] and calculate the mean potential as a function of separation distance, for three concentrations (100, 300, and 500 mM) of monovalent electrolytes. Two systems are shown in Fig. S9: one with boundaries that are dielectrically matched with the solvent (ε = 80) and a surface potential of 50 mV, and a system where the boundaries have a slightly lower dielectric constant (ε = 40) and a surface potential of 150 mV. It is clear from the results that these interaction potentials are negligible for atomistic solutes, but relevant for nanometer-sized objects; the potential increases quadratically with the size of the

object, and exceeds the thermal energy for contact areas with a radius beyond ~ 7 nm. It must be noted that a boundary with homogeneous surface charge has smaller ion-boundary correlations than a boundary with discrete surface charges. Discrete charges amplify effects like 'ion-bridging' and are expected to reduce the electrostatic repulsion, even more than in Fig. S9. At short interplate separations (< 0.78 nm), the ions are completely excluded from the confinement, resulting in a sharp collapse of the osmotic pressure. This leads to a deep potential well for salt concentrations greater than 300 mM. A similarly strong binding effect for DNA-coated AuNPs would prevent the nanoparticles from attaining the equilibrium structure of assembly. The crystal to glass transition that is observed in experiments at very high salt concentrations may be a result of such depletion-like attractions.

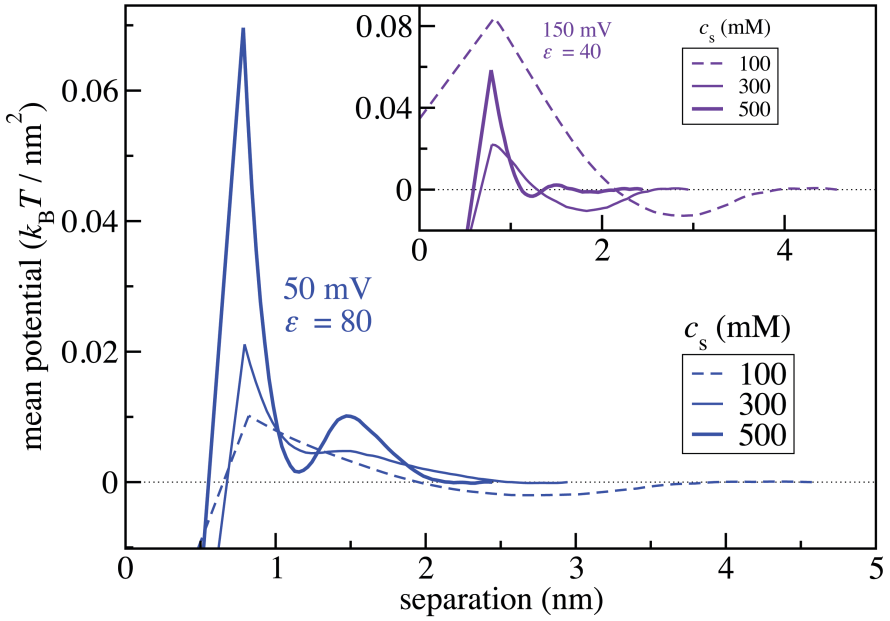

Figure S9. Mean potentials between two parallel, homogeneously charged boundaries, induced by a 1:1 aqueous electrolyte, at three different concentrations. The blue lines correspond to a system with boundaries that are dielectrically matched with the solvent, and have a surface potential of 50 mV, while the inset corresponds to a system with boundaries that have a slightly lower dielectric constant, and higher surface potential of 150 mV. The slight dielectric contrast increases the induced attractive potential significantly. The position where the ions are entirely excluded from the confinement is marked by a maximum in the potential.

8. Effective forces between functionalized nanoparticles

The average force between nanoparticles in solution results from direct physical interaction, thermal motion, and the interaction with other solutes. We estimate the strength and range of such interactions for DNA-grafted nanoparticles, in a dense solution of ions. An algebraic expression for this effective interaction can be derived from first principles, by taking the complete multi-component partition sum of nanoparticles and ions, and averaging out the degrees of freedom of the ions. We aim to keep the notation as light as possible to outline the process below. The full partition sum can be written as

$$Z\left(\mu_+, \mu_-, N_\mathrm{p}, V, T\right) = \mathrm{Tr}_\mathrm{p}\mathrm{Tr}_\mathrm{s}\,\exp\left\{-\left(U_\mathrm{pp} + U_\mathrm{ps} + U_\mathrm{ss}\right)/k_\mathrm{B}T\right\} \qquad \text{(S12)}.$$

Here, the subscript *p* refers to the nanoparticles, the subscript *s* to the salt ions. U_{ij} is the pair interaction between species *i* and *j*, and *Tr* (the 'classical trace') summarizes the integration over the degrees of freedom. By a simple reordering of integration, one can rewrite equation (S12) as

$$Z = \mathrm{Tr}_\mathrm{p}\exp\left\{-U_\mathrm{pp}/k_\mathrm{B}T\right\}\mathrm{Tr}_\mathrm{s}\exp\left\{-\left(U_\mathrm{ps} + U_\mathrm{ss}\right)/k_\mathrm{B}T\right\}$$

and define

$$\exp\left\{-U_\mathrm{mean}/k_\mathrm{B}T\right\} \stackrel{\mathrm{def}}{=} \mathrm{Tr}_\mathrm{s}\exp\left\{-\left(U_\mathrm{ps} + U_\mathrm{ss}\right)/k_\mathrm{B}T\right\} \qquad \text{(S13)}.$$

This mean potential depends explicitly on the degrees of freedom of the nanoparticles, but not on those of the salt ions, and represents an effective force that is mediated by the ions. Although the potential is in principle a many-body term that depends on the positions of all the nanoparticles, we focus on the effective interaction between two nanoparticles, assuming the pair contribution to be the dominant interaction for the moment. The evaluation of the mean potential involves a complicated high-dimensional integration, which is generally impossible to perform exactly, but can be avoided with an approximate approach that is more transparent and of general value for a broader set of interaction potentials.

To simplify the evaluation of equation (S13), we divide the system into three types of regions: I) the region where ions do not correlate with the nanoparticles (bulk solution), II) the region where ions can interact with a nanoparticle, and III) the region where ions interact with two nanoparticles. A schematic representation of this division is shown in Fig. S10.

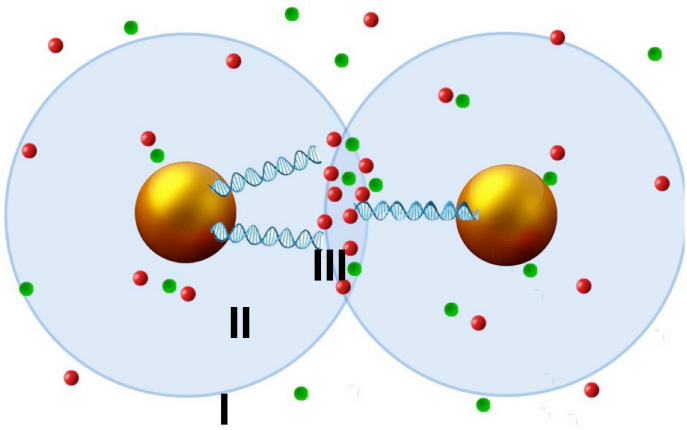

Figure S10. Schematic representation of DNA coated nanoparticles in salt solution. Three types of regions are distinguished; I) bulk solution, II) influence sphere of a nanoparticle, and III) the overlap of two influence spheres.

The 'sphere of influence' of a nanoparticle (region II) does not coincide with the hydrodynamic radius or the maximal extent of grafted chains, but rather with a larger region, that extends further over the electrostatic correlation length. This length scale ranges from a few nanometers at high salt concentrations to tens of nanometers at dilute conditions.

We can now simplify equation (S13) by evaluating the integrations within the three regions separately, ignoring boundary effects. To avoid the complications that arise when $U_{ss} \neq 0$, we substitute these pair interactions by chemical potential fields ω that we could evaluate with a field theoretical method, in principle. For the purpose of estimating the effective pair interaction it is not necessary to go into the calculation of these fields. Writing out the integration of the degrees of freedom of the salt ions,

$$\mathrm{Tr_s}\exp\left\{-\frac{(U_{\mathrm{ps}}+U_{\mathrm{ss}})}{k_{\mathrm{B}}T}\right\} =$$

$$\sum_{N_+}\frac{{z_+}^{N_+}}{N_+!}\sum_{N_-}\frac{{z_-}^{N_-}}{N_-!}\int \mathrm{d}\boldsymbol{r}^{N_+}\mathrm{d}\boldsymbol{r}^{N_-}\exp\left\{-\sum_{n=0}^{N_+}\left(\frac{U_{p+}(\boldsymbol{R_1},\boldsymbol{R_2},\boldsymbol{r}_n)}{k_{\mathrm{B}}T}+\omega_+(\boldsymbol{r}_n)\right)-\sum_{m=0}^{N_-}\left(\frac{U_{p-}(\boldsymbol{R_1},\boldsymbol{R_2},\boldsymbol{r}_m)}{k_{\mathrm{B}}T}+\omega_-(\boldsymbol{r}_m)\right)\right\} \qquad \text{S(14).}$$

The fugacity of the ions is denoted with z, and we introduce the self-consistent chemical potential fields ω that arise from ion-ion correlations. The potential U_{pi} is the direct potential between the two nanoparticles and an ion at position $\boldsymbol{r}$. The effective potential between two nanoparticles then becomes

$$U_{\mathrm{mean}}(|\boldsymbol{R}_1-\boldsymbol{R}_2|) = k_BT\sum_{i\epsilon\{+,-\}}z_i\int \mathrm{d}\boldsymbol{r}\exp\left\{-\frac{U_{pi}(\boldsymbol{R_1},\boldsymbol{R_2},\boldsymbol{r})}{k_{\mathrm{B}}T}-\omega_i(\boldsymbol{r};R)\right\} \qquad \text{(S15)}$$

with $R \equiv |\boldsymbol{R}_1-\boldsymbol{R}_2|$ the distance between the nanoparticles. Since we are aiming for a simple estimation of the order of magnitude, and a minimal description of the underlying mechanics we make the approximation that the self-consistent field is (piecewise) constant within the three regions: $\omega_+(\boldsymbol{r};R) = q_+\phi_D+\beta\mu_+^{\mathrm{exc}}$. The first constant term is the Donnan potential within the region times the charge q_+, and the second is the excess chemical potential. The Donnan potential depends on the density of charges that are bound to the nanoparticle (the grafted chains), and the excess chemical potential depends on the total density of charges within the region. Leaving out terms independent of R, we finally obtain

$$U_{\mathrm{mean}}(|\boldsymbol{R}_1-\boldsymbol{R}_2|)$$
$$= -k_BT\,V_0(|\boldsymbol{R}_1-\boldsymbol{R}_2|)\sum_{i\epsilon\{+,-\}}z_i\left(\left[e^{-\beta\mu_i^{\mathrm{exc}}}\right]_I+\left[e^{-\frac{U_{pi}}{k_{\mathrm{B}}T}-q_i\phi_D-\beta\mu_i^{\mathrm{exc}}}\right]_{III}-2\left[e^{-\frac{U_{pi}}{k_{\mathrm{B}}T}-q_i\phi_D-\beta\mu_i^{\mathrm{exc}}}\right]_{II}\right) \qquad \text{(S16)}$$

with V_0 the overlap volume of region III

$$V_o(r) = \frac{\pi}{6} D^3 \left(1 - \frac{3r}{2D} + \frac{r^3}{2D^3}\right) \quad \text{(S17)}$$

and D the diameter of the influence sphere (region II). The square brackets $[]_i$ indicate that the potentials in the Boltzmann factor apply to region i. Equation (S16) would simplify greatly for systems that contain hard spherical colloids and ideal polymer coils. The term in between the brackets would reduce to 1 in that case, and with $D = 2 \times (R_c + R_p)$, with R_c and R_p being the colloid radius and the radius of gyration for the polymer, we derive the famous Asakura-Oosawa potential.[24,25] This is an effective potential between hard colloids, driven by entropy maximization of the polymer coils. In our case, however, the effective potential contains enthalpic contributions as well, caused by ion-ion interactions (included via the excess chemical potential) and ion-nanoparticle interactions (via U_{pi} and the Donnan potential). What both situations have in common is that the total effective potential is determined by the number of mediating particles (polymers in the case of Asakura-Oosawa; ions in the current case) in the overlap volume of the influence spheres. The term within the parenthesis is generally positive because of the convexity of the Boltzmann distributions, although the potentials in region III need to be sufficiently larger than those in region II to overcome the negative term (which is generally the case, as it can be expected that both U_{pi} and Φ_D roughly double in the overlap region). For the typical parameters of DNA-grafted nanoparticles in NaCl and $CaCl_2$ solutions, one can estimate that the effective potential may exceed 1 k_BT if the concentrations are, roughly, larger than 0.1 M, such that zV_0 is of the order of unity. The overlap volume of two influence spheres that are 26 nm in diameter and separated by 23 nm (such that the overlap region is only 3 nm wide), has a volume of about 180 nm^3 and contains, at a concentration of 0.1 M, about 10 salt ions. The term in between the brackets, which represents a free energy difference per ion, only needs to be of order 0.1 to make the effective potential exceed 1 k_BT. This potential difference

can be interpreted as the sum of three separate contributions. A direct contribution is commonly referred to as 'counterion bridging', an energy gain by positioning counterions between the charged sites of two DNA chains, which is described in U_{pi}. The second contribution results from a local deformation of the ionic double layer caused by both the charged and neutral aspects of the DNA. This contribution also involves the salt ions that are not involved in the direct screening, is contained in μ^{exc}, and becomes particularly important at high concentrations. Finally, the local elevated charge density of the DNA in the overlap region changes the Donnan potential, which is felt by all the ions. These contributions generally cause attractions, as the potentials in region III typically double as compared to those in region II, and the term inside the brackets of equation (S16) increases rapidly with ion valency and concentration, because of the exponents. These arguments would apply to general classes of nanoparticles in aqueous solution, and are only distinguished by the relative magnitude of the three contributions. The highly polyvalent nature of DNA facilitates ion bridging, creates significant differences in the local Donnan potential, and affects the local structure of salt as expressed by the local chemical potential. On the basis of these estimates we expect an attractive interaction between DNA-grafted nanoparticles, induced by the ions, via ion entropy, 'ion bridges' and ionic cohesion. The analysis demonstrates that ion bridges, which are weak in monovalent electrolytes, are not a requirement for cohesive forces. A specific application of equation (S15) would deserve further study, and even the more approximate but insightful equation (S16) could be subjected to an extensive exploration of parameters, to make quantitative comparisons between different samples of nanoparticles. While the effective potential is generally attractive, the nanoparticles are stabilized by the opposing direct interaction U_{pp} (Eq. S12), which contains the steric and electrostatic repulsion between the DNA chains. This interaction increases sharply if the

nanoparticles interdigitate.

References

(1) Macfarlane, R. J.; Lee, B.; Jones, M. R.; Harris, N.; Schatz, G. C.; Mirkin, C. A. Nanoparticle Superlattice Engineering with DNA. *Science* **2011**, *334*, 204-208.

(2) Tan, S. J.; Kahn, J. S.; Derrien, T. L.; Campolongo, M. J.; Zhao, M.; Smilgies, D.-M.; Luo, D. Crystallization of DNA-Capped Gold Nanoparticles in High-Concentration, Divalent Salt Environments. *Angew. Chem., Int. Ed.* **2014**, *53*, 1316-1319.

(3) Hurst, S. J.; Lytton-Jean, A. K. R.; Mirkin, C. A. Maximizing DNA Loading on a Range of Gold Nanoparticle Sizes. *Anal. Chem.* **2006**, *78*, 8313-8318.

(4) Kewalramani, S.; Zwanikken, J. W.; Macfarlane, R. J.; Leung, C. Y.; de la Cruz, M. O.; Mirkin, C. A.; Bedzyk, M. J. Counterion Distribution Surrounding Spherical Nucleic Acid-Au Nanoparticle Conjugates Probed by Small-Angle X-Ray Scattering. *ACS Nano* **2013**, *7*, 11301-11309.

(5) Hill, H. D.; Macfarlane, R. J.; Senesi, A. J.; Lee, B.; Park, S. Y.; Mirkin, C. A. Controlling the Lattice Parameters of Gold Nanoparticle FCC Crystals with Duplex DNA Linkers. *Nano Lett.* **2008**, *8*, 2341-2344.

(6) Plimpton, S. Fast Parallel Algorithms for Short-Range Molecular-Dynamics. *J. Comput. Phys.* **1995**, *117*, 1-19.

(7) Nose, S. A Molecular-Dynamics Method for Simulations in the Canonical Ensemble. *Mol. Phys.* **1984**, *52*, 255-268.

(8) Hoover, W. G. Canonical Dynamics - Equilibrium Phase-Space Distributions. *Phys. Rev. A* **1985**, *31*, 1695-1697.

(9) Guerrero-Garcia, G. I.; Gonzalez-Mozuelos, P.; de la Cruz, M. O. Potential of Mean Force Between Identical Charge Nanoparticles Immersed in a Size-Assymetric Monovalent Electrolyte. *J. Chem. Phys.* **2011**, *135*, 164705.

(10) Allen, M. P.; Tildesley, D. J. *Computer Simulation of Liquids*; Clarendon Press: Oxford, U.K., 1989.

(11) Frenkel, D.; Smit, B.; *Understanding Molecular Simulation: From Algorithms to Applications*; Academic Press: San Diego, 2002.

(12) Clarke, A. S.; Wiley, J. D. Numerical-Simulation of the Dense Random Packing of a Binary Mixture of Hard-Spheres - Amorphous Metals. *Phys. Rev. B* **1987**, *35*, 7350-7356.

(13) Als-Nielsen, J.; McMorrow, D. *Elements of Modern X-Ray Physics*, 2nd ed.; John Wiley: Chichester, U. K., 2011.

(14) Forster, S.; Timmann, A.; Konrad, M.; Schellbach, C.; Meyer, A.; Funari, S. S.; Mulvaney, P.; Knott, R. Scattering Curves of Ordered Mesoscopic Materials. *J. Phys. Chem. B* **2005**, *109*, 1347-1360.

(15) Tinland, B.; Pluen, A.; Sturm, J.; Weill, G. Persistence Length of Single-Stranded DNA. *Macromolecules* **1997**, *30*, 5763-5765.

(16) Hagerman, P. J. Flexibility of DNA. *Annu. Rev. Biophys. Biophys. Chem.* **1988**, *17*, 265.

(17) Xiong, H. M.; van der Lelie, D.; Gang, O. Phase behavior of Nanoparticles Assembled by DNA Linkers. *Phys. Rev. Lett.* **2009**, *102*, 015504.

(18) Hill, H. D.; Macfarlane, R. J.; Senesi, A. J.; Lee, B.; Park, S. Y.; Mirkin, C. A. Controlling the Lattice Parameters of Gold Nanoparticle FCC Crystals with Duplex DNA Linkers. *Nano Lett.* **2008**, *8*, 2341-2344.

(19) Zwanikken, J. W.; Jha, P. K.; de la Cruz, M. O. A Practical Integral Equation for the Structure and Thermodynamics of Hard Sphere Coulomb Fluids. *J. Chem. Phys.* **2011**, *135*, 064106.

(20) Nightingale, E. R. Phenomenological Theory of Ion Solvation - Effective Radii of Hydrated Ions. *J. Phys. Chem.* **1959**, *63*, 1381-1387.

(21) Zwanikken, J. W.; de la Cruz, M. O. Tunable Soft Structure in Charged Fluids Confined by Dielectric Interfaces. *Proc. Natl. Acad. Sci. U. S. A.* **2013**, *110*, 5301-5308.

(22) Jing, Y. F.; Jadhao, V.; Zwanikken, J. W.; de la Cruz, M. O. Ionic Structure in Liquids Confined by Dielectric Interfaces. *J. Chem. Phys.* **2015**, *143*, 194508.

(23) Kjellander, R.; Marcelja, S. Correlation and Image Charge Effects in Electric Double Layers. *Chem. Phys. Lett.* **1984**, *112*, 49-53.

(24) Asakura, S.; Oosawa, F. On Interaction Between 2 Bodies Immersed in a Solution of Macromolecules. *J. Chem. Phys.* **1954**, *22*, 1255-1256.

(25) Asakura, S.; Oosawa, F. Interaction Between Particles Suspended in Solutions of Macromolecules. *J. Polym. Sci.* **1958**, *33*, 183-192.